COMPEL—The International Journal for Computation and Mathematics in Electrical and Electronic Engineering
Vol. 14, No. 1, 41–56 © 1995 James & James Science Publishers Ltd

THE NEAR FIELD TO FAR FIELD TRANSFORMATION

P. MONK
Department of Mathematical Sciences, University of Delaware, Newark, DE 19716, USA

(Received 9 August 1994)

ABSTRACT: If a scattering problem is solved by finite element, finite volume or finite difference methods, it is necessary to predict the far field pattern (or radar cross-section) by using a near field to far field transformation. Usually this is done using the Stratton-Chu integral relations, which give the far field pattern in terms of a near field surface integral. When volume-based methods are used this is unnatural, and it may be necessary to employ interpolation procedures to provide the necessary surface data. In this paper an alternative method based on volume integrals is proposed. The main advantage of the new procedure is that it allows the use of discrete quantities that are naturally available from the numerical scheme. However, it is now necessary to perform volume integrals. The error in the new procedure is examined, and a simple numerical example provided.

1 INTRODUCTION

If a volume-based finite element, finite difference or finite volume scheme is used to approximate an electromagnetic scattering problem, it is necessary to calculate the far field pattern (or radar cross-section) using a near to far field map. Typically, this is done using the Stratton-Chu integral formula [1]. This formula predicts the far field pattern based on integrals of the near field values on a collection surface on which both the electric and magnetic field must be known. Unfortunately, many volume-based schemes use spatially staggered grids and sometimes discontinuous basis functions. (For a selection of papers on staggered grid methods, see Refecences 2–11.) Thus an interpolation scheme may be needed to evaluate the fields on the collection surface. This problem is relatively easy to solve using structured grids (such as are used in FDTD schemes [1]), but the problem is much more difficult on unstructured tetrahedral grids. This paper proposes a new method for computing the near field to far field map based on volume integrals. There is considerable flexibility in this approach, and the error in the method is analysed to give guidelines on the choice of certain parameters. Finally, a two-dimensional example is provided to show that the method can be successful in practice.

2 TIME HARMONIC FIELDS

2.1 The Maxwell system

This section starts by describing the problem in detail, and derives the near field to far field transformation assuming that the near field is known exactly.

Suppose that there is a bounded region $\Omega \subset \mathbb{R}^3$ such that in the exterior of Ω the electromagnetic field is propagating in free space, where the electromagnetic parameters are assumed to be $\epsilon = \mu = 1$. Thus, if $E(x,t)$ denotes the scattered electric field at position $x \in \mathbb{R}^3$ and time t, and if $H(x,t)$ denotes the scattered magnetic field,

$$E(x,t) = \hat{E}(x)e^{-ikt} \quad \text{and} \quad H(x,t) = \hat{H}(x)e^{-ikt}$$

where k is a real wave number and $i = \sqrt{-1}$. Then, by assumption, in $\mathbb{R}^3\backslash\bar{\Omega}$ (where $\bar{\Omega}$ denotes the closure of Ω), the function $\hat{E}$ and $\hat{H}$ satisfy the Maxwell system

$$-ik\hat{E} - \nabla \times \hat{H} = 0 \qquad \text{in } \mathbb{R}^3\backslash\bar{\Omega} \tag{1a}$$

$$-ik\hat{H} + \nabla \times \hat{E} = 0 \qquad \text{in } \mathbb{R}^3\backslash\bar{\Omega} \tag{1b}$$

In addition the field is assumed to satisfy the Silver–Muller radiation condition, which states that, if $r = |x|$,

$$\lim_{r\to\infty} (\hat{E} \times x + r\hat{H}) = 0 \qquad \text{uniformly in } \hat{x} = \frac{x}{|x|} \tag{2}$$

Because $\hat{E}$ and $\hat{H}$ satisfy the homogeneous Maxwell system 1 away from boundaries, we can assume that $\hat{E}$ and $\hat{H}$ are continuously differentiable solutions of equations 1 and 2. Furthermore, because $\hat{E}$ and $\hat{H}$ are radiating, it is known [12] that, for large $r = |x|$, the fields have the form

$$\hat{E}(x) = \frac{e^{ik|x|}}{|x|}\left\{\hat{E}_\infty(\hat{x}) + O\left(\frac{1}{|x|}\right)\right\} \tag{3a}$$

$$\hat{H}(x) = \frac{e^{ik|x|}}{|x|}\left\{\hat{H}_\infty(\hat{x}) + O\left(\frac{1}{|x|}\right)\right\} \tag{3b}$$

where $\hat{x} = x/|x|$, and $\hat{E}_\infty$ and $\hat{H}_\infty$ are the electric and magnetic far field patterns (from which the radar cross-section can be calculated). The problem is to provide a useful formula for $\hat{E}_\infty$ and $\hat{H}_\infty$. The details of the scattering problem satisfied by $\hat{E}$ and $\hat{H}$ in Ω can be ignored.

Let D_R be a domain with the inner boundary being the boundary of Ω (or, more precisely, the outer boundary of Ω) and the outer boundary the surface of the sphere of radius R. The boundary of D_R at $|x| = R$ is denoted by Γ_R. Now let ψ be a continuously differentiable cut-off function that satisfies the following conditions:

- $\psi = 0$ *in the neighbourhood of* Ω
- $0 \leqslant \psi(x) \leqslant 1$ for all $x \in \mathbb{R}^3$
- $\psi(x) = 1$ if $|x| \geqslant R'$, where $R' < R$

An example of a suitable function ψ is given later. For convenience, the support of $\psi(1-\psi)$ is denoted by S so that

$$S = \{x \in \mathbb{R}^3 \mid \psi(x) \neq 0 \quad \text{and} \quad \psi(x) \neq 1\}$$

By these assumptions, S is bounded and the boundary of S is disjoint from the boundary of Ω.

Theorem 2.1 Under the conditions on $\hat{E}$, $\hat{H}$ and ψ presented above,

$$\hat{E}_\infty(\hat{x}) = \frac{ik}{4\pi} = \int_S [\hat{x} \times (\nabla\psi(y) \times \hat{E}(y)) - \hat{x}(\hat{E}(y) \cdot \nabla\psi(y)) + (\nabla\psi(y) \times \hat{H}(y))] e^{-ik\hat{x}\cdot y} \, dV(y) \tag{4}$$

Remarks

1. A similar formula holds for H_∞.
2. $\hat{x} \cdot E_\infty(\hat{x}) = 0$. This implies cancellation of radial terms in the integral.

Proof Let $C^m(D)$ denote the set of m times continuously differentiable functions on a domain D. The generalized Stratton-Chu formula [12: p. 149, theorem 6.1] states that if $u \in C^1(D_R) \cap C(\bar{D}_R)$ and $v \in C^1(D_R) \cap C(\bar{D}_R)$ then, for any $x \in D_R$,

$$\begin{aligned} u(x) = & -\nabla_x \times \int_{\partial D_R} (\nu(y) \times u(y)) \Phi(x,y) \, ds(y) \\ & + \nabla_x \int_{\partial D_R} \nu(y) \cdot u(y) \Phi(x,y) \, dA(y) \\ & - ik \int_{\partial D_R} \nu(y) \times v(y) \Phi(x,y) \, dA(y) \\ & + \nabla_x \times \int_{D_R} \{\nabla \times u - ikv\}(y) \Phi(x,y) \, dV(y) \\ & - \nabla_x \int_{D_R} (\nabla \cdot u)(y) \Phi(x,y) \, dV(y) + ik \int_{D_R} \{\nabla \times v + iku\}(y) \Phi(x,y) \, dV(y) \end{aligned} \tag{5}$$

where ν is the unit outward normal to D_R and Φ is the fundamental solution of the Helmholtz equation given by

$$\Phi(x,y) = \frac{1}{4\pi} \frac{e^{ik|x-y|}}{|x-y|} \qquad x \neq y$$

Let $u = \hat{E}\psi$ and $v = \hat{H}\psi$ in equation 5 and assume $|x| > R'$ so that $u(x) = \hat{E}(x)\psi(x) = \hat{E}(x)$. Then using the fact that $\psi(x) = 0$ on $\partial\Omega$ and $\psi(x) = 1$ on Γ_R in equation 5 gives

$$\hat{E}(x) = -\nabla_x \times \int_{\Gamma_R} (\nu(y) \times \hat{E}(y))\, \Phi(x,y)\, dA(y)$$

$$+ \nabla_x \int_{\Gamma_R} \nu(y) \cdot E(y)\, \Phi(x,y)\, dA(y) - ik \int_{\Gamma_R} (\nu(y) \times \hat{H}(y))\, \Phi(x,y)\, dA(y) \tag{6}$$

$$+ \nabla_x \times \int_{D_R} (\nabla \times (\psi \hat{E}) - ik\psi \hat{H})(y)\, \Phi(x,y)\, dV(y)$$

$$- \nabla_x \int_{D_R} \nabla \cdot (\psi \hat{E})(x)\, \Phi(x,y)\, dV(y) + ik \int (\nabla \times (\psi \hat{H}) + ik\psi \hat{E})\, \Phi(x,y)\, dV(y)$$

Using the facts that $\psi = 1$ or 0 on $\mathbb{R}^3 \backslash \bar{S}$ and that $\hat{E}$ and $\hat{H}$ satisfy equations 1,

$$\nabla \times (\psi \hat{E}) - ik\psi \hat{H} = \begin{cases} \nabla\psi \times \hat{E} & \text{in } S \\ 0 & \text{otherwise} \end{cases}$$

$$\nabla \times (\psi \hat{H}) + ik\psi \hat{E} = \begin{cases} \nabla\psi \times \hat{H} & \text{in } S \\ 0 & \text{otherwise} \end{cases}$$

Equation 1a implies (because $k \neq 0$) that $\nabla \cdot \hat{E} = 0$ in $\mathbb{R}^3 \backslash \bar{\Omega}$, so

$$\nabla \cdot (\psi \hat{E}) = \begin{cases} \nabla\psi \cdot \hat{E} & \text{in } S \\ 0 & \text{otherwise} \end{cases}$$

Using these expressions in equation 6 and letting R increase without bound, it can be shown that

$$\hat{E}(x) = \nabla_x \times \int_S \nabla\psi(y) \times \hat{E}(y) \Phi(x,y)\, dV(y)$$

$$- \nabla_x \int_S \nabla\psi(y) \cdot \hat{E}(y)\, \Phi(x,y)\, dV(y) + ik \int_S \nabla\psi(y)$$

$$\times \hat{H}(y) \Phi(x,y)\, dV(y) \tag{7}$$

(Because $\hat{E}$ and $\hat{H}$ satisfy equation 2 and Φ satisfies the Sommerfeld radiation condition, the integrals on Γ_R in equation 6 vanish as R increases [12: pp. 154–155].)

Finally, letting $|x| \to \infty$ in equation 7 and using the fact that $E(x)$ behaves as in equation 3a, together with standard estimates for the asymptotic behaviour of Φ and its derivatives [12], gives equation 4 from equation 7. □

2.2 The Helmholtz equation

An expression similar to equation 6 can also be obtained for the Helmholtz equation. Supposing that $\hat{u}(x)$ satisfies the Helmholtz equation

$$\Delta\hat{u} + k^2\hat{u} = 0 \quad \text{in} \quad \mathbb{R}^3 \backslash \bar{\Omega} \tag{8}$$

where $\Omega \subset \mathbb{R}^3$ is a bounded domain, and that $\hat{u}$ satisfies the Sommerfeld radiation condition

$$\lim_{r \to \infty} r\left(\frac{\partial \hat{u}}{\partial r} - ik\hat{u}\right) = 0 \tag{9}$$

then (see, for example, Reference 12) $\hat{u}(x)$ has a a well defined far field pattern $\hat{u}_\infty(\hat{x})$ defined by

$$\hat{u}(x) = \frac{e^{ik|x|}}{|x|}\left\{\hat{u}_\infty(\hat{x}) + O\left(\frac{1}{|x|}\right)\right\}$$

Again the problem is to compute the far field pattern $\hat{u}_\infty(x)$ from a knowledge of near field values of $\hat{u}$ in the vicinity of Ω.

Let $\psi \in C^2(\mathbb{R}^3)$ be a cut-off function satisfying the conditions given in the previous subsection; then we have the following theorem.

Theorem 2.2 Let $\hat{u}$ be a solution of equations 8 and 9. Then

$$\hat{u}_\infty(\hat{x}) = -\frac{1}{4\pi}\int_S \hat{u}(y)\,(-\Delta\psi + 2ik\hat{x}\cdot\nabla\psi)\,(y)\,e^{-ik\hat{x}\cdot y}\,dV(y) \tag{10}$$

Remark Integrating the term $u\Delta\psi$ by parts gives the equivalent formula

$$\hat{u}_\infty(\hat{x}) = -\frac{1}{4\pi}\int_S (-\Delta\hat{u} + ik\hat{u}\hat{x})\,(y)\cdot\nabla\psi(y)\,e^{-ik\hat{x}\cdot y}\,dV(y) \tag{11}$$

or, integrating by parts further,

$$\hat{u}_\infty(\hat{x}) = -\frac{1}{4\pi}\int_S (\hat{u}\Delta\psi + 2\nabla\psi\cdot\nabla\hat{u})\,(y)\,e^{-ik\hat{x}\cdot y}\,dV(y) \tag{12}$$

Equation 10 has the advantage that no derivatives of u are required, but a smoother function ψ is needed.

Proof The proof follows along the same lines as the previous proof.

First it is necessary to prove equation 12. If D_R is the same domain as in the previous proof, then for $x \in D_R$ theorem 2.1 on p. 16 of Reference 12 shows that for any function $v \in C^2(D_R) \cap C(\bar{D}_R)$ the following identity holds:

$$v(x) = \int_{\partial D_R} \frac{\partial v}{\partial \nu}(y)\,\Phi(x,y) - v(y)\frac{\partial \Phi}{\partial \nu(y)}(x,y)\,dA(y)$$

$$-\int_{D_R}(\Delta v + k^2 v)\,(y)\,\Phi(x,y)\,dV(y)$$

Now choose $v = \hat{u}\psi$ and assume $|x| > R'$. Of course $\hat{u}$ has the necessary smoothness because it satisfies a homogeneous Helmholtz equation in the region of interest. Using the fact that $\Delta\hat{u} + k^2\hat{u} = 0$ in D_R, $\psi = 1$ on Γ_R and $\hat{u}\psi = 0$ on $\partial\Omega$ gives

$$\hat{u}(x) = \int_{\Gamma_R} \frac{\partial \hat{u}}{\partial \nu}(y)\,\Phi(x,y) - \hat{u}(y)\frac{\partial \Phi}{\partial \nu}(x,y)\,dA(y)$$

$$-\int_{D_R}(\hat{u}\Delta\psi + 2\nabla\hat{u}\cdot\nabla\psi)\,(y)\,\Phi(x,y)\,dV(y)$$

Now, letting $|x| \to \infty$ and using the radiation condition 9 (satisfied by $\hat{u}$ and Φ) together with the asymptotics of Φ for large arguement proves equation 12.

Applying integration by parts to the term $\nabla\psi \cdot \nabla\hat{u}$ gives

$$\hat{u}_\infty(x) = -\frac{1}{4\pi}\int_S \hat{u}[\Delta\psi e^{-ik\hat{x}\cdot y} - 2\nabla(e^{-ik\hat{x}\cdot y}\nabla\psi)]\,dV(y)$$

$$= -\frac{1}{4\pi}\int_S \hat{u}(-\Delta\psi + 2ik\hat{x}\cdot\nabla\psi)e^{-ik\hat{x}\cdot y}\,dV(y)$$

which is exactly equation 10. □

In the analogue of equation 10 for $\mathbb{R}^2$, the fundamental solution is

$$\Phi(x,y) = \frac{i}{4}H_0^{(1)}(k|x-y|) \qquad x \neq y$$

and using this in the previous proof together with standard asymptotic approximations of the first kind Hankel function for larae argument gives the following results.

Theorem 2.3 If u satisfies equations 8 and 9 in $\mathbb{R}^2$, then

$$\hat{u}_\infty(x) = -\frac{e^{i\pi/4}}{\sqrt{(8\pi k)}}\int_S \hat{u}(y)(-\Delta\psi + 2ik\hat{x}\cdot\nabla\psi)(y)e^{-ik\hat{x}\cdot y}\,dA(y) \tag{13}$$

Analogues for equations 11 and 12 also hold.

2.3 Construction of ψ

There is considerable flexibility in constructing ψ. This section suggests a moderately general ψ, and a two-dimensional analogue of this choice of ψ is used in Section 5.

Let $\phi_0(r)$ be the quintic B-spline with knots at $x = 0,1,2,3,4,5$ and 6 normalized so that $\phi_0(3) = 11/20$. Then let

$$\psi_1(r) = \begin{cases} 0 & \text{if } r \leqslant 0 \\ \phi_0(r) + \phi_0(r+1) + \phi_0(r+2) + \phi_0(r+3) + \phi_0(r+4) & \text{if } 0 \leqslant r \leqslant 5 \\ 1 & \text{if } r \geqslant 5 \end{cases}$$

Because it is a quintic spline, $\psi_1 \in C^4(\mathbb{R})$ and $\psi_1^{(5)}$ is piecewise constant. Now let A be a 3×3 non-singular matrix and let $r_{\max} > r_{\min} > 0$ and

$$\psi(x) = \psi_1(5(\|Ax\| - r_{\min})/(r_{\max} - r_{\min})) \tag{14}$$

This function has the property that

$$\psi(x) = \begin{cases} 0 & \text{if } \|Ax\| \leqslant r_{\min} \\ 1 & \text{if } \|Ax\| \geqslant r_{\max} \end{cases}$$

Furthermore, $\|Ax\| = r$ implies that $x^T A^T Ax = r^2$ and thus, $\|Ax\| = r$ is an ellipsoid in $\mathbb{R}^3$. Choosing A and $r_{\min}$ so that $\|Ax\| = r_{\min}$ contains $\bar{\Omega}$ in its interior, $r_{\max}$ can be chosen to adjust the volume of the collection domain S. With this construction, S is just the ellipsoidal shell $r_{\min} \leqslant \|Ax\| \leqslant r_{\max}$.

$\nabla\psi$ and $\Delta\psi$ are easy to compute:

$$\nabla\psi(x) = \hat{\psi}'(S(x))\left(\frac{5}{r_{\max} - r_{\min}}\right)\frac{A^T Ax}{\|Ax\|} \tag{15}$$

where $S(x) = 5(\|Ax\| - r_{\min})/(r_{\max} - r_{\min})$. In the same way,

$$\Delta\psi(x) = \hat{\psi}''(s(x))\left(\frac{5}{r_{\max} - r_{\min}}\right)^2 \frac{\|A^T Ax\|^2}{\|Ax\|^2}$$
$$+ \left(\hat{\psi}'(s(x))\frac{tr(A^T A)}{\|Ax\|} - \hat{\psi}'(S(x))\frac{\|A^T Ax\|}{\|Ax\|^3}\right)\left(\frac{5}{r_{\max} - r_{\min}}\right) \tag{16}$$

Similar expressions can be given for higher derivatives.

3 TIME-DEPENDENT PROBLEMS

To solve the time-dependent Maxwell system (for example, using finite-element time domain methods), the time-dependent scattered electric field $E(x,t)$ and magnetic field $H(x,t)$ are assumed to satisfy

$$\frac{\partial E}{\partial t} - \nabla \times H = 0 \qquad \text{in } \mathbb{R}^3\backslash\bar{\Omega} \tag{17a}$$

$$\frac{\partial H}{\partial t} + \nabla \times E = 0 \qquad \text{in } \mathbb{R}^3\backslash\bar{\Omega} \tag{17b}$$

and the field is assumed to be outgoing so that, at the initial time $t = 0$,

$$E(x,0) = H(x,0) = 0 \qquad \text{for all } x \in \mathbb{R}^3\backslash\bar{\Omega}$$

This implies that the scattered field originates inside Ω, so that the Fourier transform of the fields (which is assumed to exist) given by

$$\hat{E}(x) = \frac{1}{\sqrt{(2\pi)}}\int_{-\infty}^{\infty} E(x,t)\,e^{ikt}\,dt$$

$$\hat{H}(x) = \frac{1}{\sqrt{(2\pi)}}\int_{-\infty}^{\infty} H(x,t)\,e^{ikt}\,dt$$

satisfies equations 1 and 2. Thus, $\hat{E}_\infty(x)$ is given by Theorem 2.1. Now taking the inverse Fourier transform of equation 4 and defining

$$E_\infty(\hat{x},t) = \frac{1}{\sqrt{(2\pi)}}\int_{-\infty}^{\infty} \hat{E}_\infty(\hat{x},k)\,e^{-ikt}\,dt$$

(where it has been explicitly shown that $\hat{E}_\infty$ depends on k), gives

$$E_\infty(\hat{x},t) = -\frac{1}{4\pi}\int_S \hat{x} \times (\nabla\psi(y) \times E_t(y,t + \hat{x}\cdot y))$$
$$- \hat{x}\nabla\psi(y)\cdot E_t(y,t + \hat{x}\cdot y) + (\nabla\psi(y) \times H_t(y,t + \hat{x}\cdot y))\,dV(y) \tag{18}$$

Even if the time harmonic far field pattern is needed, it may be preferable to compute the time-dependent response using equation 18 and the Fourier transform $E_\infty(x,t)$ to get the time-harmonic response.

For the wave equation, a similar time-dependent far field pattern is obtained by taking the Fourier transform of 10. Under the conditions of Theorem 2.2, defining

$$u(x,t) = \frac{1}{\sqrt{(2\pi)}} \int_{-\infty}^{\infty} \hat{u}(x)\, e^{-ikt}\, dk$$

gives

$$u_\infty(x,t) = -\frac{1}{4\pi} \int_S u(y,t + \hat{x}\cdot y)\, \Delta\psi(y) + 2\nabla u(y,t+\hat{x}\cdot y)\cdot\nabla\psi(y)\, dV(y) \quad (19)$$

Similar expressions hold for the time-dependent versions of equations 11 and 12.

4 ANALYSIS OF THE METHOD

There are three sources of error in computing the far field pattern by any method:

- Perturbation of the underlying problem
- Numerical solution of the perturbed problem
- Numerical evaluation of the near to far field map

The time-harmonic Helmholtz problem discussed in Section 2.2 will be analysed in this section.

To use finite element, volume or difference methods it is usual to introduce an artificial boundary and then solve the Helmholtz equation 8 on the bounded domain with a suitable absorbing boundary condition on the artificial boundary. Let $\hat{u}$ be the exact solution of the time-harmonic problem (as in Section 2.2), $\hat{u}_{ABC}$ the exact solution of the perturbed problem with the absorbing boundary condition, and $\hat{u}^h_{ABC}$ the finite difference, volume or element approximation to $\hat{u}_{ABC}$. Then the numerical far field pattern is approximated by using equation 10 on the numerical solution $\hat{u}^h_{ABC}$ with the integral replaced by quadrature.

Usually the quadrature on S will be a composite quadrature rule. This means that S is covered with a mesh of elements of maximum diameters h (usually the mesh used to compute $\hat{u}^h_{ABC}$). Let us denote the mesh on S by τ_h so that τ_h is the set of all elements with non-zero intersection with S. An element $K\in\tau_h$ will usually be either a cuboid or a tetrahedron but could be more complex. On each element $K\in\tau_h$, p-point quadrature is used with quadrature points a_i^K, $1\leqslant i\leqslant p$ and weights w_i^K, $1\leqslant i\leqslant p$. Thus the numerical approximation to $u_\infty(\hat{x})$ will be

$$\hat{u}^{h,Q}_{ABC,\infty}(\hat{x}) = -\sum_{K\in\tau_h}\sum_{j=1}^{p} \frac{w_i^K}{4\pi} [\hat{u}^h_{ABC}(a_i^K)(-\Delta\psi + 2ik\hat{x}\cdot\nabla\psi)(a_i^K)]e^{-ik\hat{x}\cdot a_i^K} \quad (20)$$

Denoting by $\hat{u}_{ABC,\infty}(\hat{x})$ the right-hand side of equation 10 with $\hat{u}$ replaced by $\hat{u}_{ABC}$, and by $\hat{u}^h_{ABC,\infty}(\hat{x})$ the right-hand side with $\hat{u}$ replaced by $\hat{u}^h_{ABC}$, the total pointwise error in the far field pattern is

$$\hat{u}_\infty(\hat{x}) - \hat{u}^{h,Q}_{ABC,\infty}(\hat{x}) = (\hat{u}_\infty(x) - \hat{u}_{ABC,\infty}(\hat{x})) + (\hat{u}_{ABC,\infty}(\hat{x}) - \hat{u}^h_{ABC,\infty}(\hat{x})) + (\hat{u}^h_{ABC,\infty}(\hat{x}) - \hat{u}^{h,Q}_{ABC,\infty}(\hat{x})) \tag{21}$$

The first term on the right-hand side is the error due to the absorbing boundary condition. This depends on the absorbing boundary condition in use and is not discussed further here. The next term on the right-hand side of equation 21, $\hat{u}_{ABC,\infty} - \hat{u}^h_{ABC,\infty}$, is due to the error in solving the perturbed problem numerically with the given absorbing boundary condition. Typically, if the absorbing boundary condition does not introduce singularities in the solution, this term can be controlled by a careful choice of the mesh. The final term on the right-hand side of equation 21 is due to the discretization of equation 10 via numerical quadrature and will be discussed in some detail next.

For simplicity, let us assume that $\hat{u}^h_{ABC}$ is a continuous piecewise degree l finite element function. Thus $\hat{u}^h_{ABC}$ is continuous and, on each element $K \in \tau_h$, $\hat{u}^h_{ABC}|_K$ is a polynomial of degree l. The error $\hat{u}^h_{ABC,\infty} - \hat{u}^{h,Q}_{ABC,\infty}$ is due to quadrature error as follows:

$$\hat{u}^h_{ABC,\infty}(\hat{x}) - \hat{u}^{h,Q}_{ABC,\infty}(\hat{x}) = \frac{-1}{4\pi}\left[\sum_{K\in\tau_h}\left\{\int_K \hat{u}^h_{ABC}(y)\left(-\Delta\psi(y) + 2ik\hat{x}\cdot\nabla\psi(y)\right)e^{-ik\hat{x}\cdot y}\,dV(y) - \sum_{j=1}^{p} w^K_L\left[\hat{u}^h_{ABC}(a^K_i)\left(-\Delta\psi + 2ik\hat{x}\cdot\nabla\psi\right)\right](a^K_i)\,e^{-ik\hat{x}\cdot a^K_i}\right\}\right]$$

Now suppose that

$$\int_K \phi(y)\,dV(y) = \sum_{j=1}^{p} w^K_j \phi(a_j)$$

for all polynomials ϕ of degree less than or equal to $2l$ in the three variables x,y,z. Then, provided the mesh is regular and quasi-uniform, the quadrature estimates for finite element methods in theorem 4.1.5 of Reference 13 show that

$$\left|\hat{u}^h_{ABC,\infty}(\hat{x}) - \hat{u}^{h,Q}_{ABC,\infty}(\hat{x})\right| \leqslant Ch^{l+1}\left\|\left(-\Delta\psi + 2ik\hat{x}\cdot\nabla\psi\right)e^{-ik\hat{x}\cdot y}\right\|_{l+1}\left\|\hat{u}^h_{ABC}\right\|_1$$

where $\|\cdot\|_m$ is the mth order Sobolev norm on the domain S [14]. Because $O(h^{l+1})$ convergence for $\hat{u}^h_{ABC}$ in the L^2 norm is expected, this choice of quadrature order implies that, for fixed ψ and k, optional order convergence from the quadrature will be obtained.

For constant k,

$$\left\|\left(-\Delta\psi + 2ik\hat{x}\cdot\nabla\psi\right)e^{-ik\hat{x}\cdot y}\right\|_{l+1} \leqslant C\|\psi\|_{l+3}$$

The norm of ψ depends on $\hat{\psi}$, the matrix A and the constants $r_{\max}$ and $r_{\min}$ if ψ is constructed by the method outlined in Section 2.3. In particular, if A and $\hat{\psi}$ are

fixed, and $r_{\max} - r_{\min}$ is small, derivations like those leading to equations 15 and 16 show that

$$\|\psi\|_{l+3} \leqslant \frac{C(\hat{\psi},A)}{(r_{\max} - r_{\min})^{l+3}}$$

where $C(\hat{\psi},A)$ is a constant depending on $\hat{\psi}$ and A. It is of particular interest to obtain $O(h^2)$ convergence, so that $l = 1$. Then

$$|\hat{u}^h_{ABC,\infty}(\hat{x}) - \hat{u}^{h,Q}_{ABC,\infty}(\hat{x})| \leqslant C\frac{h^2}{(r_{\max} - r_{\min})^4} \tag{22}$$

The point of this estimate is that, if $r_{\max} - r_{\min} = O(h)$, there is no approximation in the quadrature estimate. In other words, the domain S must contain a number of layers of elements in order to approximate the far field pattern well. The dependency of the far field pattern on $r_{\max} - r_{\min}$ is investigated in Section 5.

5 NUMERICAL RESULTS

These results are intended to investigate the dependence of the error in the computed far field pattern on the parameters $r_{\max}$ and $r_{\min}$. A simple example of the use of the technique on a scattering problem is also provided.

To compute the far field pattern due to the scattering of an incident plane wave from a hard circular cylinder, let $W = \{x \in \mathbb{R}^2 \mid |x| \leqslant 0.1\}$. Then the scattered field satisfies the following system of equations:

$$\Delta\hat{u} + k^2\hat{u} = 0 \qquad \text{in } \mathbb{R}^2 \backslash W \tag{23a}$$

$$\frac{\partial\hat{u}}{\partial r} = -\frac{\partial}{\partial r} e^{ikx} \qquad \text{on } \partial W \tag{23b}$$

$$\frac{\partial\hat{u}}{\partial r} + ik\hat{u} = o\left(\frac{1}{r^{1/2}}\right) \qquad \text{uniformly as } r \to \infty \tag{23c}$$

This problem is easy to solve using standard special functions, which allow the computation of $\hat{u}$ and $\hat{u}_\infty$ accurately to check predicted far field patterns.

5.1 Exact data

To investigate how the error in the computed far field pattern depends on the cut-off function ψ, we compute near field data $\hat{u}$ exactly using the special function solution of equation 23. In particular, suppose that $\hat{u}$ is known at the centroid of each triangle in the unstructured mesh shown in Figure 1. This mesh covers the annulus

$$D_A = \{x \in \mathbb{R}^2 \mid 0.1 < |x| < 0.6\}$$

Thus we can apply equation 13 using the two-dimensional cut-off function described in Section 2.3 by taking A to be the identity matrix and $0.1 \leqslant r_{\min} < r_{\max} \leqslant 0.6$.

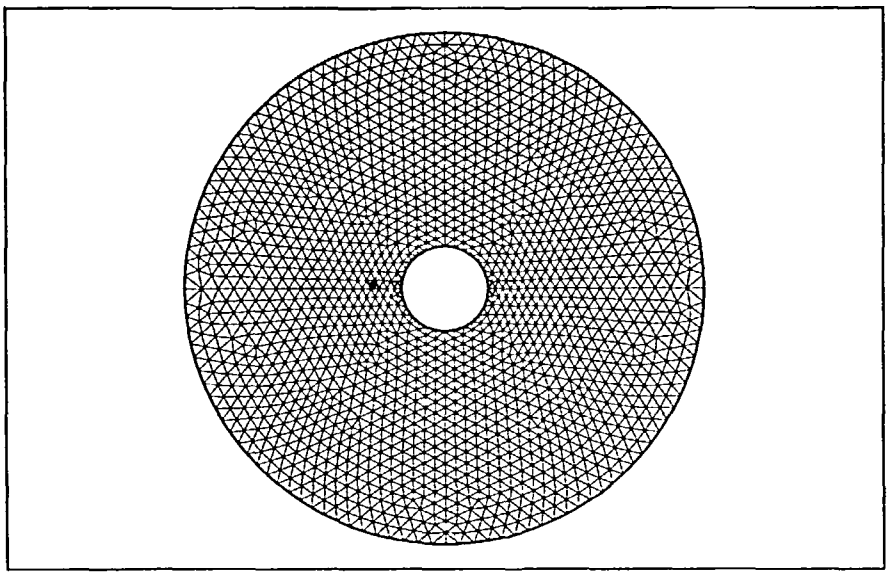

Figure 1 The finite element mesh used in this paper. The mesh covers the annular region $0.1 \leqslant |x| \leqslant 0.6$. The inner circle is a perfectly conducting object, and the outer circle is an absorbing boundary given by equation 27.

Because the data is known at the centroid of each element, the midpoint quadrature formula can be used, so that, if K is a triangle and f a function,

$$\int_K f(x)\,\mathrm{d}A \approx \mathrm{area}(K) f(x_C)$$

where x_C is the centroid of the triangle. This rule is accurate for linear polynomials, so $l = 1$ as in equation 22. Using this quadrature to approximate equation 13 on each triangle gives a two-dimensional version of equation 20 that will be used in this section.

Define the maximum norm relative error in the far field pattern by

$$\|\hat{u}_\infty - \hat{u}^{h,Q}_{ABC,\infty}\| = \frac{\max_{|\hat{x}|=1} |\hat{u}_\infty(\hat{x}) - \hat{u}^{h,Q}_{ABC,\infty}(\hat{x})|}{\max_{|\hat{x}|=1} |\hat{u}_\infty(\hat{x})|}$$

In practice, the maximum is computed by examining the far field patterns at 360 equally spaced points on the unit circle.

Figures 2 and 3 show the relative L^2 error in the far field pattern for $k = 10$ (Figure 2) and $k = 20$ (Figure 3) as a function of the size of the annulus S given by $r_{\max} - r_{\min}$ for $r_{\min} = 0.1$ and $0.15 \leqslant r_{\max} \leqslant 0.6$. Clearly the error decreases as $r_{\max} - r_{\min}$ increases, and the slope of the error curve is initially approximately -4 as predicted. The error decrease reaches a plateau at a relative error of approximately 0.07% for $k = 10$ and 0.11% for $k = 20$. This error is due to the quadrature and given mesh, because only the quadrature error term contributes in equation 21. With exact data, the only requirement for an accurate solution is for $r_{\max} - r_{\min}$ to be large enough (and of course for the mesh to be fine enough for accurate integration). The best choice is for both $r_{\min}$ and the region S to be as small as possible, so that the number of triangles processed is as small as possible.

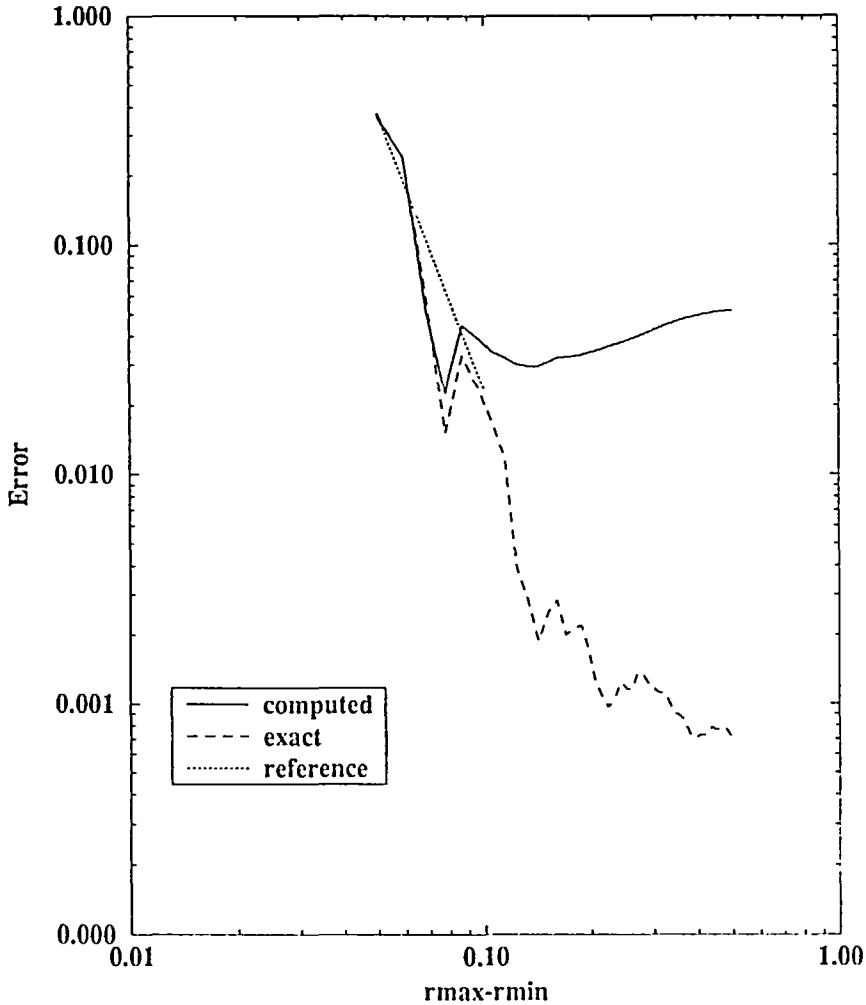

Figure 2 The relative error in the far field pattern as a function of $r_{max} - r_{min}$ when exact and computed data is used (at the centroid of each triangle in the mesh in Figure 1). Data for wave number $k = 10$, $r_{min} = 0.1$ and $0.15 \leqslant r_{max} \leqslant 0.6$ is shown. The line labeled 'computed' is the error using finite element time domain data; the 'exact' curve is the error using data generated by the series solution of the problem, including error due to quadrature. In both cases the error decreases at approximately fourth order (shown by the reference line) for small values of $r_{max} - r_{min}$, as expected from theory. The error in the 'computed' value rises as r_{max} approaches the outer boundary, which may be caused by the use of an approximate absorbing boundary condition.

5.2 Numerical data

The example in Section 5.1 was intended to demonstrate the behaviour of the method as certain parameter values are varied. This section investigates a model problem using approximate time-dependent data to compute an approximate fixed frequency far field pattern. The problem is two-dimensional and there are better ways to solve the problem

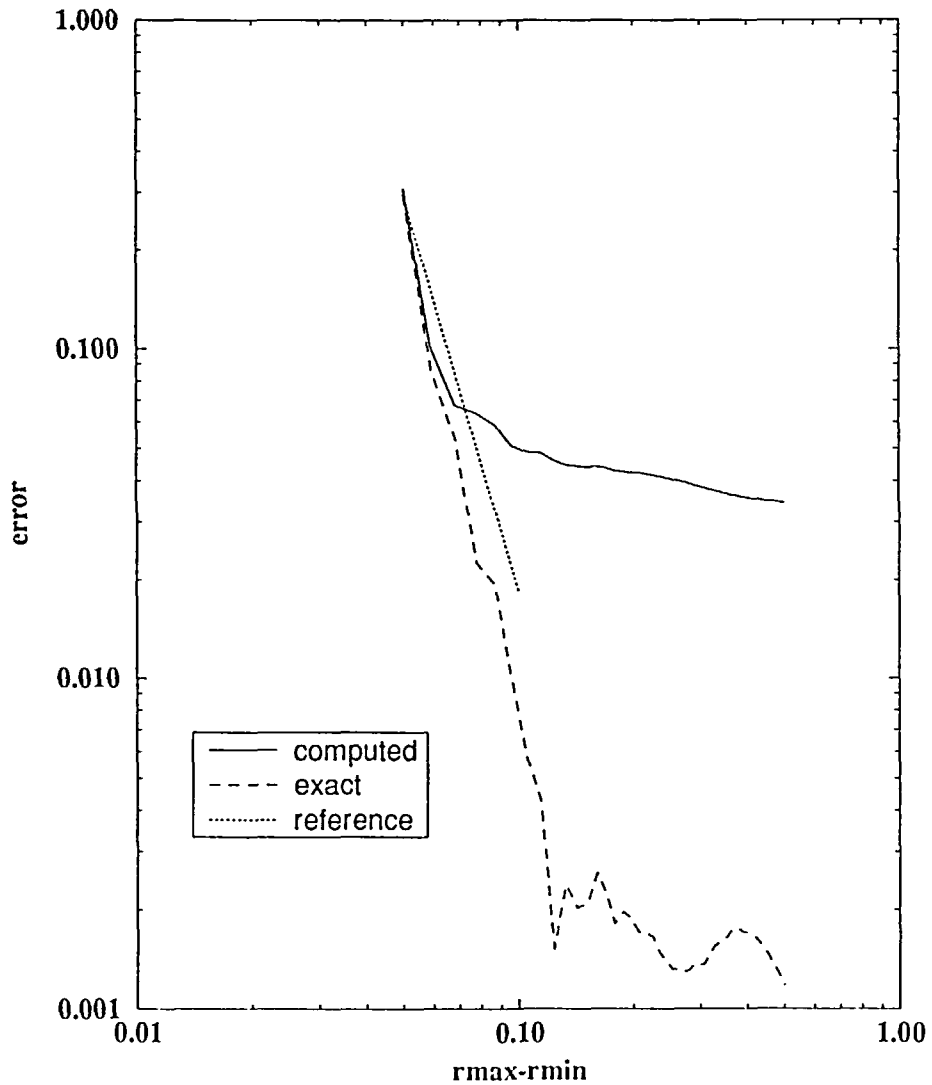

Figure 3 The relative error in the far field pattern as a function of $r_{max} - r_{min}$ when computed and exact data are used (at the centroid of each triangle in the mesh in Figure 1). Data for wave number $k = 20$, $r_{min} = 0.1$ and $0.15 \leqslant r_{max} \leqslant 0.6$ is shown. At first the error decreases, as is expected from the previous computation, and a good estimate of the far field pattern is obtained when $r_{max} - r_{min} = 0.1$, which uses 672 triangles of a possible 3272. Using the optimal value of r_{max} the relative error using exact data is 0.11% (this error is due to quadrature error alone) and 3.4% using finite element data from the time-dependent finite element computation.

than the one used here, but it illustrates the overall technique in a verifiable setting. The problem is to compute a fixed frequency far field pattern of a perfectly conducting infinite circular cylinder of radius 0.1 due to plane wave excitation.

The time-dependent scattered near field data is approximated by solving the two-dimensional Maxwell system

$$\epsilon_0 \frac{\partial E}{\partial t} - \vec{\nabla} \times H = 0 \qquad \text{in } D_A \tag{24a}$$

$$\mu_0 \frac{\partial H}{\partial t} + \nabla \times E = 0 \qquad \text{in } D_A \tag{24b}$$

where $D_A = \{x \in \mathbb{R}^2 | 0.1 < |x| < 0.6\}$, $\epsilon_0 = 8.85 \times 10^{-3}$, $\mu_0 = 1.2566 \times 10^3$ and

$$\vec{\nabla} \times H = \begin{pmatrix} \frac{\partial H}{\partial y} \\ -\frac{\partial H}{\partial x} \end{pmatrix} \qquad \nabla \times E = \frac{\partial E_2}{\partial x} - \frac{\partial E_1}{\partial y}$$

The initial data is

$$H(x,0) = 0 \quad \text{and} \quad E(x,0) = 0 \tag{25}$$

Because the cylinder is assumed to be perfectly conducting, the boundary data on the inner boundary is

$$\nu \times E = -\nu \times E^i \quad \text{for} \quad |x| = 0.1 \tag{26}$$

where E^i is the Gaussian plane wave:

$$E^i = \begin{pmatrix} 0 \\ \sqrt{\left(\frac{\mu_0}{\epsilon_0}\right)}\, g(t - [x - 0.1]\sqrt{[\epsilon_0 \mu_0]}) \end{pmatrix}$$

and $g(s) = \exp(-10(s-1)^2)$. We use the simplest absorbing boundary condition

$$E \times \hat{x} + \sqrt{\left(\frac{\mu_0}{\epsilon_0}\right)} H = 0 \qquad \text{on} |x| = 0.6 \tag{27}$$

The initial boundary value problem (equations 24–27) is approximated using linear Nédélec edge elements [15,8] on the mesh in Figure 1 and time stepped using leapfrog time stepping with a time step of 0.01. The result of this computation is an approximation to $H(x,t)$ at the centroid of each triangle in the mesh shown in Figure 1 for $0 \leqslant t \leqslant 5$. Taking the Fourier transform by approximating the required integral numerically, it is possible to compute

$$\hat{H}(x,\omega) = \frac{1}{\sqrt{(2\pi)}} \int_{-\infty}^{\infty} H(x,t)\, e^{i\omega t}\, dt$$

and

$$\hat{g}(x,\omega) = \frac{1}{\sqrt{(2\pi)}} \int_{-\infty}^{\infty} g(t - \sqrt{[\epsilon_0 \mu_0]}0.1)\, e^{i\omega t}\, dt$$

Then $\hat{u} = \hat{H}/\hat{g}$ satisfies equation 23 approximately provided $k = \sqrt{(\epsilon_0 \mu_0)}\omega$. Thus, for any given k, it is possible to approximate $\hat{u}$ at the centroid of each triangle in the mesh and to compute the approximate fixed frequency far field pattern. The error in this computed far field pattern includes all types of error discussed in Section 4 (equation 21).

Figures 2 and 3 show the relative maximum norm error in the computed far field pattern for $k = 10$ and $k = 20$ as a function of $r_{max} - r_{min}$ with $r_{min} = 0.1$ and $0.15 \leqslant r_{max} \leqslant 0.6$ using computed data. At first the error decreases, as is expected from the previous example, but for $k = 10$ (Figure 2) the error increases as the outer edge of the annulus approaches the artificial boundary. Using the value of $r_{max} - r_{min} \approx 0.08$, the relative error is 2% when $k = 10$ and 6% when $k = 20$. (When $k = 20$, the choice $r_{max} - r_{min} \approx 0.5$ gives the better error of about 3.4%.) Compared with using exact near field data, the finite difference time domain solution has introduced extra discretization error.

6 CONCLUSION

A new method for computing the far field pattern from near field values is proposed and analysed. This method is well suited to numerical data arising from edge finite element methods on unstructured grids. The major disadvantage is the need to handle volume data (or, in two dimensions, area data) to compute the far field pattern. To apply this method to the full Maxwell system in $\mathbb{R}^3$, the design of a cut-off ψ function to minimize the volume of the integration region S is of particular importance.

ACKNOWLEDGEMENTS

This research was supported in part by AFOSR.

REFERENCES

1. Taflove, A. and Umashankar, K. Radar cross section of general three-dimensional scatterers. *IEEE Trans.* **EMC-25** (1983) 433-440.
2. Yee, K. Numerical solution of initial boundary value problems involving Maxwell's equations in isotropic media. *IEEE Trans.* **AP-16** (1966) 302-307.
3. Shankar, V., Hall, W. and Mohammadian, A. A time-domain differential solver for electromagnetic problems. *Proc. IEEE* **77** (1989) 709-721.
4. Rappaport, C. FDTD analysis of electromagnetic scattering in anisotropic media unconstrained triangular meshes. *IEEE Trans.* **AP-39** (1991) 345-349.
5. Mur, G. The finite-element modeling of three-dimensional time-domain electromagnetic fields in strongly inhomogeneous media. *IEEE Trans.* **MAG-28** (1992) 1130-1133.
6. Cioni, J., Fezoui, L. and Steve, H. A parallel time-domain Maxwell solver using upwind schemes and triangular meshes. *Impact of Computing in Science and Engineering* **5** (1993) 215-247.
7. Makridakis, C. and Monk, P. Time-discrete finite element schemes for Maxwell's equations. *Math. Model. Numer. Anal.* (1995) in press.
8. Monk, P. and Parrott, A. A dispersion analysis of finite element methods for Maxwell's equations. *SIAM J. Sci. Stat. Comput.* SIAM J Scientific Computing **15** (1994) 916-937.
9. Lee, J.-F. Solving Maxwell's equations by finite element time domain methods (1995), in press.
10. Mahadevan, K., Mittra, R. and Vaidya, P.M. Use of Whitney's edge and face elements for efficient finite element time domain solution of Maxwell's equations. *Journal of Electromagnetic Waves and Applications*, **8** (1994) 1173-1191.
11. Mahadevan, K. and Mittra, R. Radar cross section computations of inhomogeneous scatterers using edge-based finite element method in frequency and time domains. *Radio Science* **28** (1993) 1181-1193.

12. Colton, D. and Kress, R. *Inverse Acoustic and Electromagnetic Scattering Theory*. Springer-Verlag, New York (1992).
13. Ciarlet, P. *The Finite Element Method for Elliptic Problems*. Vol. 4 of *Studies In Mathematics and Its Applications*. Elsevier North-Holland, New York (1978).
14. Adams, R. *Sobolev Spaces*. Vol. 65 of *Pure and Applied Mathematics*. Academic Press, New York (1975).
15. Nédélec, J. Mixed finite elements in $\mathbb{R}^3$. *Numer. Math.* **35** (1980) 315–341.